Synthesis of TiO$_2$/Cellulose Nanocomposites and its Application for Degradation of Methylene Blue

[1,*]Tran Thi Bich Quyen, [2]Phan Van Hoang Khang, [3]Ngo Nguyen Tra My and [4]Doan Van Hong Thien,
[1,2,3,4]Department of Chemical Engineering, College of Technology, Can Tho University, 3/2 Street, Ninh Kieu District,
Can Tho City, Vietnam
*Corresponding Author: Tran Thi Bich Quyen

Abstract: TiO$_2$/cellulose nanocomposites (TiO$_2$/NC NCPs) have been successfully synthesized using natural sources from sugarcane bagasse and titanium butoxide precursors'. The obtained results from Field Emission Scanning Electron Microscopy (FESEM) and Transmission Electron Microscopy (TEM) micrographs show that the TiO$_2$/NC NCPs particles with average size respective ~4.5-10 nm (TiO$_2$ nanoparticle) and ~10-25 nm (cellulose nanorectangular) are distributed well and homogeneous. Besides, X – ray Diffraction (XRD) displays nanocellulose (NC) which is high crystallinity (~77%) and nanotitanium dioxide (NT) is anatase phase. Energy Dispersive X-ray Spectrometry (EDX) spectra demonstrates that NT exists in the samples. The band-gap of new material also is decreased, which allows to enhance photocatalytic ability. Moreover, TiO$_2$/cellulose nanocomposites are used as nanomaterials with high photocatalytic and adsorption ability for degradation of methylene blue (MB) under support of the sunlight and hydroxy peroxide. The decompositional yield of MB reaches up to 98.3% within 90 min. Last but not least, the material also can be reused simply to decaying MB with 3 cycles.

Keywords: *TiO$_2$/cellulose nanocomposites (TiO$_2$/NC NCPs); photocatalysis; degradation of methylene blue (MB); sugarcane bagasse; cellulose nanorectangular.*

I. INTRODUCTION

In recent years, nanocellulose (NC) have been used as a sustainable carbohydrate polymer material in numerous innovative electronics for their quintessential features such as flexibility, low thermal expansion and self-/directed assembly within multiphase matrices. NC is natural material, a cheap and sustainable polymeric material with useful functional properties such as tailored hydro/oleophilicity, optical transparency and remarkable mechanical performance both as films and aerogels [1-7]. The exploration of cellulose nanoparticle hybrids is still relatively sparse but has increased pronouncedly since the pioneering report on multifunctional magnetic NC hybrids.

Nanotitanium dioxie, especially the anatase form of TiO$_2$ that has more oxygen vacancies than the rutile phase, has a high photocatalytic efficiency under UV light [8]. For anatase TiO$_2$, its (001) facet has a higher surface energy of 0.90 J/m^2 than other facets, thus a highest chemical activity [9-11]. Titania-based materials are very attractive due to their inherent high refractive index and UV absorbing properties. For instance, titania-polymer hybrids have been prepared with conductive polymers [12-14], polyacrylonitrile electrospun fibers [15], polyacrylonitrile and carbon nanotubes [16,17], block co-polymers [18–20], polystyrene beads [21, 22], polyamide [23], acrylic acid or PMMA [24–26], silicates or siloxanes [27], polyimides [28], epoxies [29], and polycations [30].

Organic–inorganic nanocomposites or hybrids have attracted much interest due to their current and potential applications as they can combine useful chemical, optical and mechanical characteristics [31, 32]. Traditionally, organic–inorganic nanocomposites have had a focus on the polymeric matrix, being e.g., formed from vinyl polymers, condensation polymers or polyolefins filled with relatively passive inorganic components such as layered silicates, i.e., montmorillonite or hectorite [31, 32]. With the strong movement towards biodegradable, renewable, sustainable, and carbon-neutral polymeric materials, it is also of importance to develop viable and facile production routes for nanocomposites using such biopolymers.

In this work, we report the facile fabrication of TiO$_2$/cellulose nanocomposite hybrids with high inorganic content by the adsorption of TiO$_2$ (anatase) nanoparticles on plant-derived rectangular cellulose nanocrystals. The nanostructure of the hybrids was characterized mainly by electron microscopy and the optical transparency and mechanical performance of the hybrids were evaluated using spectrophotometry and nanoindentation tests, respectively.

II. MATERIALS AND METHODS

a. Materials

Ethanol (C$_2$H$_5$OH; 96%), Sodium hydroxide (NaOH; 99%), Sulfuric acid (H$_2$SO$_4$; 98%), Acetic Acid (CH$_3$COOH; 99%), Sodium hypochlorite (NaClO; 99%), Titanium Butoxide (Ti(Obu)$_4$; 99%), Ethylene Glycol (C$_2$H$_4$(OH)$_2$; 99%), Ammonium Chlorite (NH$_4$Cl; 99%), Methylene Blue (C$_{16}$H$_{18}$ClN$_3$S. xH2O; 99%), and Hydroxy Peroxide (H$_2$O$_2$; 30%) were bought from Sigma-Aldrich. A local sugar factory located Can Tho city, Vietnam, supplied sugarcane bagasse. All solutions were prepared with deionized water from a MilliQ system.

b. Preparation of cellulose

A local sugar factory located Can Tho city, Vietnam, supplied sugarcane bagasse. After drying and grinding, sugarcane bagasse was refluxed in Soxhlet apparatus with C$_2$H$_5$OH and DI H$_2$O with ratio 1:1 (v/v). Next to, the deposit was treated with a solution of H$_2$SO$_4$ 5%, NaOH 5%, mixture between NaClO 5% and a few drops of CH$_3$COOH, NaOH 18%, respectively. Finally, the product was dried in vacuo oven at 60°C, 0.03 MPa for 6 h to obtain purified cellulose.

c. Preparation of cellulose nanorectangular

0.5 g purified cellulose was stirred with 20 mL H$_2$SO$_4$ solution with speed is 1000 rpm *(Table 1)*. To recrystallize nanocellulose (NC), 200 mL cold DI H$_2$O was added into the above solution mixture. The mixture was centrifuged for several times in order to remove excess acid. Pre-product was sonicated for 1 h in an ice bath to avoid overheating and dried

in vacuum oven at 60°C, 0.03 MPa in 12 h, respectively. NC powder was stored at 2°C for next steps.

d. Synthesis of TiO$_2$ nanoparticles

The different volumes (0.25, 0.5 and 0.75 mL) of (Ti(Obu)$_4$ were dropped slowly into 5 mL C$_2$H$_4$(OH)$_2$ during 20 min. Those were stirred homogeneously by heating a magnetic stirrer to form a gel. After that, the gel was poured into a 100 mL solution of 3.5 g NH$_4$Cl dissolved carefully in H$_2$SO$_4$ 0.1 M. The reaction was carried out during 1 h at 90°C. A milky solution was centrifuged a lot of times and dried in vacuo oven at 24 h, 60°C and 0.03 MPa to obtain white nanopowder (TiO$_2$ nanoparticles: NT).

e. Preparation of TiO$_2$/cellulose nanocomposites

0.5 g NT was added into a beaker containing 200 mL H$_2$SO$_4$ 0.1 M. The suspension was sonicated 15 min in ice bath. Next, 10, 15, 20 and 25 mL solutions of NC 2% were poured NT solution mentioned, respectively. The absorption process between NC and NT happened at 40°C for 4 h and stirred at 800 rpm. When the one stopped, TiO$_2$/cellulose nanocomposites (TiO$_2$/NC NCPs) solution was neutralized by NaOH 0.1 M. The mixture was decanted of the clear water and centrifuged repeatedly to obtain the samples. The suspension was dried in vacuum oven at 60°C for 24 h and 0.03 MPa to get TiO$_2$/NC NCPs powder.

f. Preparation of methylene blue solution

Weighing various sample weights put into a beaker of methylene blue (MB) 40 ppm solution with a few drops of H$_2$O$_2$ and sonicated in an ice bath for 7 min. Then, It was placed under sunlight (13 p.m) to degrade the contaminants. On the other hand, a control examination between NC, NT, TiO$_2$/NC NCPs and without the catalyst also proceeded. And then, the material as soon as treatment was separated by centrifugation within 2 min. A detailed way of the experiments as shown in *Table 2*. Amount of lost MB was determined according to *Equation 1*.

$$H\% = 100 \cdot (C/C_o) \; (Equation\ 1)$$

where $\Delta C = C_o - C$.
C$_o$: original MB concentration
C: remain MB concentration

g. Reusing of TiO$_2$/cellulose nanocomposites after adsorbing and photocatalytic methylene blue

Weighing and adding TiO$_2$/cellulose nanocomposites (TiO$_2$/NC NCPs) into MB 40 pm solution (without H$_2$O$_2$), TiO$_2$/NC NCPs was sonicated within 7 min. Then, it was exposed to sunlight at 13 p.m. Optimum conditions are results of the above experiments. After the processing time has elapsed, the material was centrifuged for 2 min. Then, they were soaked in C$_2$H$_5$OH for 15 min and gone on centrifuging to wash off the solvent. This process was repeated several times until removing absolutely the adsorbed pigments on the surface. Finally, TiO$_2$/NC NCPs were washed once with distilled water and vacuum dried within 12 h at 0.03 MPa, 60°C. The reusing process was carried out 3 times.

III. RESULTS AND DISCUSSION

Table 1 illustrates the yield of isolation NC. Namely, the highest mass is No.1 with 72.38%. Follow that, No.5, No.2 and No.3 are 61.14%, 41.9% and 41.7%, respectively. The quantity of both No.6 and No.7 is insignificant with 0.74% and 3.2%, respectively. Finally, recrystallization does not happen according to No.4 and No.8 possibly due to large acidic

concentration and high temperature. Meanwhile, cellulose molecules will be depolymerized quickly in a strong acidic environment to form an oligomer solution [33]. Hence, the best optimum condition for isolation NC is 50% H$_2$SO$_4$ at 30°C within 30 min.

Table 1. Conditions and results nanocellulose isolation

No	Conc. H$_2$SO$_4$ (%)	Temp. ($^{\circ}$C)	Time (min)	Yield (%)
1	50	30	30	72.38
2	55	30	30	41.9
3	50	45	30	41.7
4	55	45	30	0
5	50	30	45	61.14
6	55	30	45	0.74
7	50	45	45	3.12
8	55	45	45	0

NT has linked with NC via hydro linkage. The volume ratio between two ones plays a vital role in enhancing absorption intensity of UV-vis spectrum (Figure 1). In fact, the sample comprises 10 mL of NC solution, the maximum absorption peak is 346 nm. Compared with the sample containing 15 mL, this value is larger up to 395 nm belonging to the UVA region. However, according to 20 mL and 25 mL of NC solution, they tend to transfer to the UVB region with 380 and 376 nm, respectively. Band gap energy is determined according to *Equation 2*.

$$E(eV) = (1239.8)/\lambda \; (nm) \; (Equation\ 2)$$

where λ(nm) is maximum absorption wavelength.

The change of band gap energy corresponding to each various NC volume is demonstrated in Figure 2. The band gaps of NC solutions (10 mL, 15 mL, 20 mL and 25 mL) were obtained correspond to 3.58 eV, 3.14 eV, 3.26 eV and 3.3 eV, respectively. Band gap energy is widened when overloading possibly due to aggregation of NC in an acid environment. To sum up, this hybrid material improves photocatalytic capacity and as well as restricting recombination of electrons and holes.
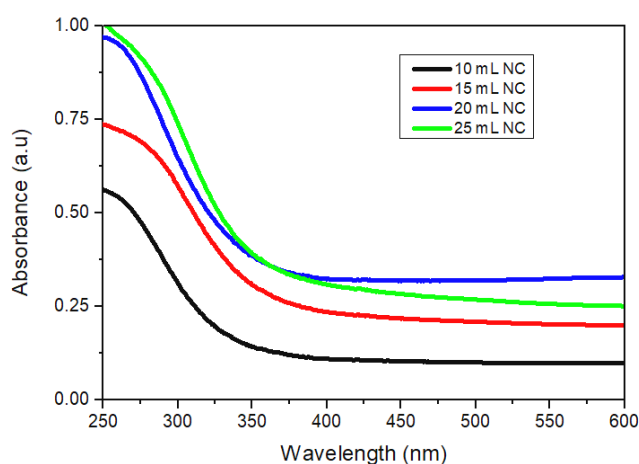
Figure 1. UV-vis spectras of TiO$_2$/cellulose nanocomposites with various volumes of nanocellulose.
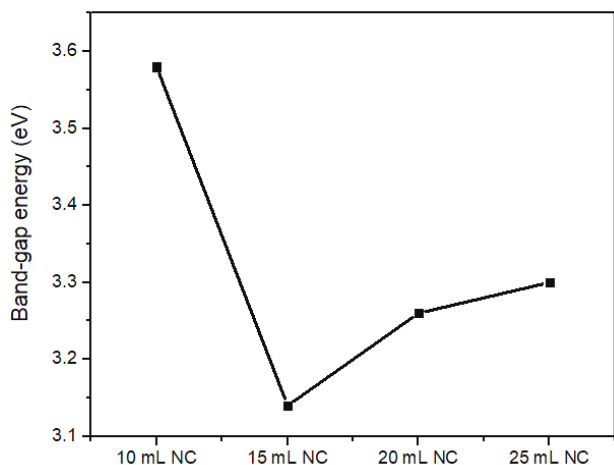
Figure 2. Bandgap energy of TiO$_2$/cellulose nanocomposites.

The lattice structure of both NC and TiO$_2$/NC NCPs as shown in Figure 3. Specific peaks of NC appear at 12°, 20°, 22°, and 34° correspoding with planes (101), (100), (002) and (040) verify high crystallinity. Peaks of 2θ = 20°, 22° and 34° represent for both type (I) and (II) of cellulose while 2θ = 12° is feature signal of only type (II) off cellulose [34, 35]. Cellulose type (I) exists in almost all planes and is able to be transferred to type (II) by NaOH and H$_2$SO$_4$. Hydroxyl groups are changed by ONa$^-$ groups in the alkaline process. Thence, when centrifugation and washing off by DI H$_2$O, ions' Na$^+$ is separated leading to cellulosic type II generated. When presenting NT, special peaks intensity are decreased strongly possibly due to "covering phenomenon". Moreover, feature peaks' anatase phase also are bared on XRD pattern at 2θ = 25°, 2θ = 38°, 2θ = 47°, 2θ = 54° and 2θ = 62° assigning as facets of (101), (004), (200), (105), (211) and (213).
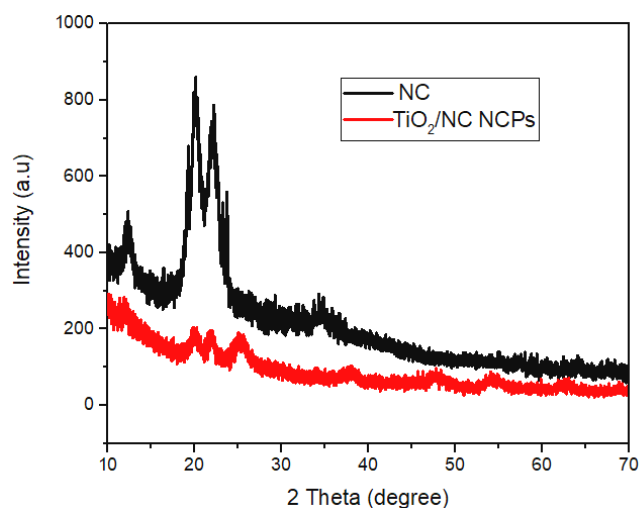
Figure 3. XRD patterns of TiO$_2$/cellulose nanocomposites and nanocellulose.

Informationally chemical groups and its transformation when adding NT solutions is recorded by the FTIR spectrum (Figure 4). Firstly, in NC the control sample, featuring vibrations in range 3175 – 3440 cm^{-1} are assigned to intermolecular O-H of type I cellulose stretching. Bands 2730 – 2910 cm^{-1}, 1640 – 1660 cm^{-1}, 1443-1458 cm^{-1}, 1370-1380 cm^{-1} are assigned C-H stretching, O-H bending due to absorbed water [36], CH$_2$ in cellulose scissoring motion and C-H bending, respectively. Peaks at 1332 cm^{-1}, 1313 cm^{-1} and 1250 cm^{-1} are assigned O-H bending, CH$_2$ wagging and C-O outside aryl ring out of lignin bended. Even though sugarcane bagasse has retreated well, lignin molecules are still present due to

recombination in order to form suspensive products. Furthermore, peak at 1054 cm^{-1} (C-O-C ring pyranose stretching), and band at 892 – 900 cm^{-1} (present cellulosic β-glycosidic linkage), peaks at ~1125 cm^{-1} (C-C ring stretching band) and 1105 cm^{-1} (C-O-C glycosidic linkage of ether) also are observed [37-39]. Peaks 1430 cm^{-1} and 893 cm^{-1} are out of type I cellulose type [40]. Besides that, a strong peak at 1375 cm^{-1}, two weak peaks at 1335 cm^{-1} and 1313 cm^{-1} and a slight band at 1275 – 1285 cm^{-1} diffused other spectral bands at 1100 cm^{-1} also are assigned to cellulose type I [41]. Secondly, as far as TiO$_2$/NC NCPs, although feature spectral bands are into NC still appearance, the spectral intensity is decreased significantly due to "covering phenomenon". Especially, bands at 3175 and 3440 cm^{-1} being O-H bending because it is blocked by titanium via Ti-O-Cellulose linkage.
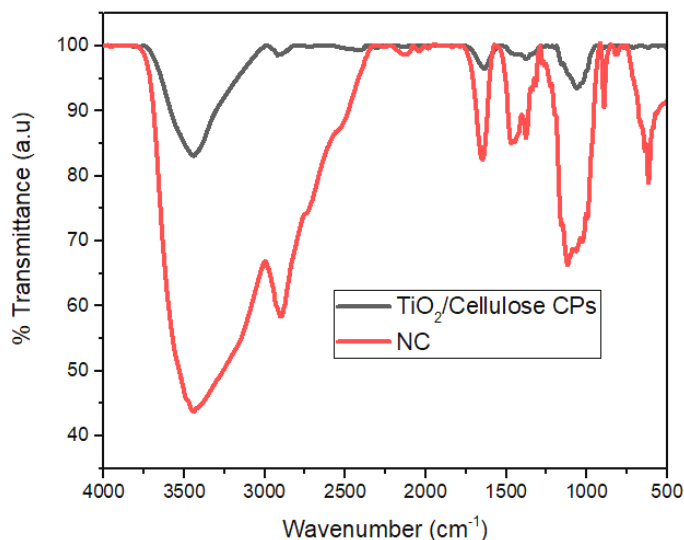
Figure 4. FTIR spectras of TiO$_2$/cellulose nanocomposites (c) and nanocellulose.

The morphology of TiO$_2$/NC NCPs is shown in Figure 5. Surface s' TiO$_2$/NC NCPs have a lot of porosity and NT is dispersed well on the NC surface (Figure 5a). Polymerization between NT and NC creates a scabrous surface, hence, it also possesses high potential adsorption. However, they tend to be aggregated because of hydro linkages. TEM image (Figure 5b) displayed that the NC is rectangular with a length of 20–30 nm and a width of 10-25 nm. Besides, the NT is spherical nanoparticles which is the range size ~4.5 – 10 nm. Furthermore, TEM image in Figure 5(b) also shown those both of them are adsorbed on the mutual surface. This result is suitable with both FTIR spectrums and XRD patterns.

(a)

(b)
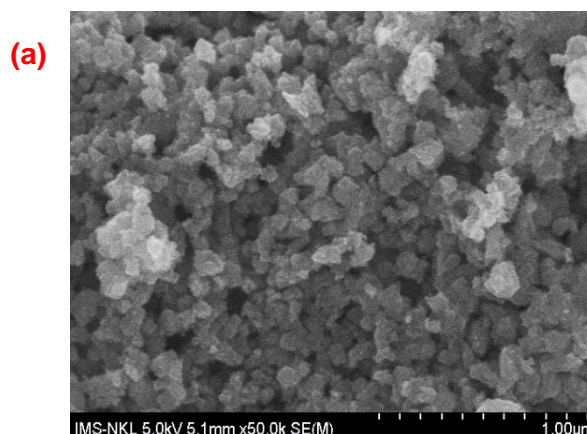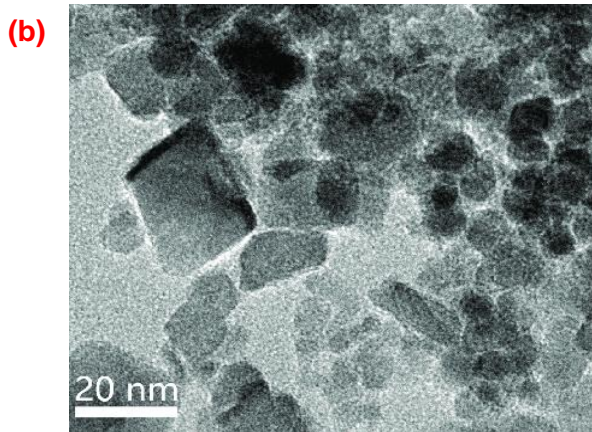
Figure 5. (a) FESEM and (b) TEM images of TiO₂/cellulose nanocomposites, respectively.

EDX which is attached to FESEM was used for elemental analysis of TiO₂/NC NCPs. In EDX spectra (Figure 6), there are peaks of carbon, oxygen, sodium, sulfur and titanium. Hydrogen s' peaks are absent since there is a slight atom. TiO₂/NC NCPs compose of 1.11% và 0.91% impurities of sodium and sulfur, respectively, because of esterification of the NC surface. In the other hand, main atoms include of 30.59% carbon, 48.24% oxygen and 19.16% titanium as shown in Figure 6.
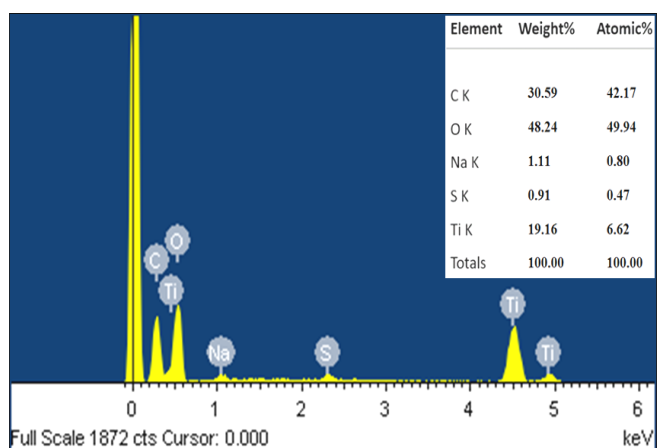
Figure 6. EDX spectrum of TiO₂/cellulose nanocomposites.

The result methylene blue (MB) disintegration is shown as in Figure 7 and Table 2. First of all, to prove MB dye degradation by TiO₂/NC NCPs, symmetric experiments between TiO₂/NC NCPs, NCs, NTs and without catalysts were carried out. From the obtained results (Figure 7a), TiO₂/NC NCPs show that MB dye decomposition is better than others by virtue of the combination of adsorption and photocatalytic. The TiO₂/NC NCPs degrade MB solution is 98.3% higher than those of NTs, NCs and the blank sample respective being 86.7%, 79.6% and 58.4% for comparisons. According to NCs, the adsorption of NCs is dominant while NTs are photocatalytic. However, the recombination of electrons and holes in NTs leads to lower the yield. As far as the blank sample, the lost MB comes to the hydroxyl group (OH.) generated by decaying of the H_2O_2 under the ultraviolet radiation but not significantly. It indicated that H_2O_2 plays a secondary role in the break up of MB dye while the catalyst is a key factor. Results as shown in Figure 7(b), when reaction time is increased from 30, 60 to 90 min, MB percentages also go up from 79.2% to 90.4% and up to 97.2%, respectively. However, within 120 min, this line is flat because of the saturated solution and covered the catalyst's surface by pollutant. Various mass effects of the material are significantly

different to degradation of MB dye. And the catalytic efficiency of TiO₂/NC NCPs for the degradation of MB dye correspond 58.3%, 89.9%, 91.4% and 89.8% when the amount of TiO₂/NC NCPs were used respective being 0 mg, 25 mg, 50 mg and 75 mg. When overloaded mass, below materials are unable to be exposed to photons to generate pairs of the electron and holes.

Table 2. Conditions and yield of degradation methylene blue

Factor	No	Study Condition	Degraded Percentage (%)
Role of TiO₂/NC NCPs	1	TiO₂/NC NCPs	98.3
	2	NT	86.7
	3	NC	79.6
	4	Blank	58.4
Time	1	30 min	79.2
	2	60 min	90.4
	3	90 min	97.2
	4	120 min	97.2
Mass TiO₂/NC NCPs	1	0 g	58.3
	2	0.0025 g	89.9
	3	0.005 g	91.4
	4	0.0075 g	89.8
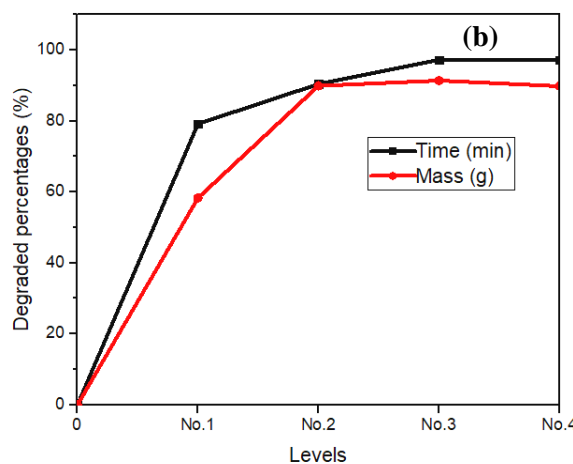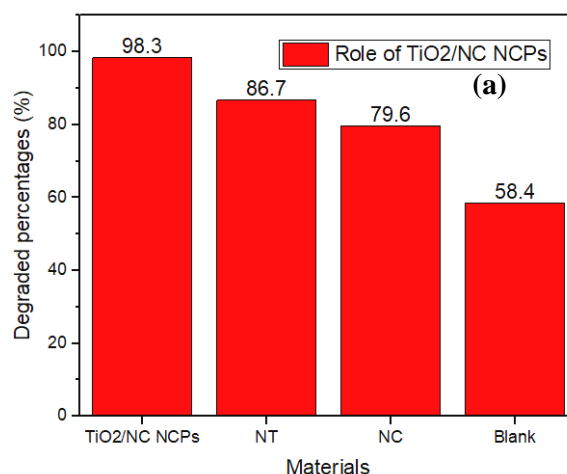
Figure 7. (a) Comparison of TiO₂/NC nanocomposites and other catalysts (b) yields of decaying methylene blue corresponding various times and weights

Nanocomposites' TiO₂/NC NCPs are able to redo for 3 times (Figure 8). In the first cycle, the yield rises steadily from 30, 60 to 90 min corresponding to 86.4%, 88.5% and 91.9% according to sample comprises TiO₂/NC NCPs, respectively.

As far as samples without the material, within 90 min, MB only loses 8.1 %. The next cycle, we can also observe differences between both two ones. In the blank sample, MB percentages are decomposed by sunlight within 30, 60 and 90 min increases linearly, respective being 4.3%, 12.6% and 18.9%. Even higher than the first cycle a little, it is not crucial possibly due to different radiation between days. Collating it with the control sample, it is lower significantly. Namely, at 30 min, 60 min and 90 min, respectively, the yield is 84.5%, 83.8% and 82.1%. Compared to the control sample in the first cycle, they slightly decrease because of TiO$_2$/NC NCPs surface covered by pigment. Following this, TiO$_2$/NC NCPs cannot be exposed to sunlight to create pairs of electrons and holes as well as receiving pollutants on the facets. The final cycle, percentages' MB decomposed go down only 68.3% after 30 min and improve up to 73.6% and 74% within the next 30 min and 60 min. After two cycles, on the TiO$_2$/NC NCPs' surface, there are a lot of MB adsorbed so that TiO$_2$/NC NCPs cannot react to the sunlight to generate hydroxyl groups. From the above result evidented that TiO$_2$/NC NCPs possess highly potential ability in order to redo to decompose the MB. Besides, this material can easily recover by simple methods. Thus, it promises to become an elite catalyst applied in various fields.

Figure 8. Recycling of TiO$_2$/cellulose nanocomposites

CONCLUSIONS

Methylene Blue is a carcinogenic dye and one of the environmental pollutants. Herein, we fabricated successfully a hybrid nanocomposite between NCs (~10-25 nm with nanorectangular morphology) and NTs (~4.5-10 nm), for removal of the MB from aqueous solution. Structure, properties, morphology and ingredients are characterized by FESEM, TEM, XRD, FTIR, UV-vis and EDX analyses. They are carried out to explore the optimum conditions of time and mass make significant contributions in treatment contaminants for the dye removal.. TiO$_2$/NC NCPs show good photocatalytic and adsorption recyclability. Thus, it is an elite material for the degradation of MB dye from aqueous solution and can be applied as an assistance for the removal of MB dye from industrial effluents.

References

[1]. Klemm D, Kramer F, Moritz S, Lindstro ̈m T, Ankerfors M, et al. (2011) NCs: A new family of nature-based materials. Angew Chem Int Ed 50: 5438–5466.

[2]. Gross RA, Kalra B (2002) Biodegradable polymers for the environment. Science 297: 803–807.

[3]. Beecher JF (2007) Organic materials: Wood, trees and nanotechnology. Nat Nanotechnol 2: 466–467.

[4]. Isogai A, Saito T, Fukuzumi H (2011) Tempo-oxidized cellulose nanofibers. Nanoscale 3: 71–85.

[5]. Sehaqui H, Salajkova M, Zhou Q, Berglund LA (2010) Mechanical performance tailoring of tough ultra-high porosity foams prepared from cellulose i nanofiber suspensions. Soft Matter 6: 1824–1832.

[6]. Sehaqui H, Zhou Q, Ikkala O, Berglund LA (2011) Strong and tough cellulose nanopaper with high specific surface area and porosity. Biomacromolecules 12: 3638–3644.

[7]. Cervin NT, Aulin C, Wa ̊gberg L, Larsson T (2011) Hydrophobic aerogels from nanofibrillated cellulose (nfc) with tunable oleophilicity. In: Abstracts of Papers of the American Chemical Society. P.241.

[8]. Xie, G. et al. Graphene-Based Materials for Hydrogen Generation from Light-Driven Water Splitting. Advanced Materials. 25, 3820–3839 (2013).

[9]. Han, X., Kuang, Q., Jin, M., Xie, Z. & Zheng, L. Synthesis of Titania Nanosheets with a High Percentage of Exposed (001) Facets and Related Photocatalytic Properties. Journal of the American Chemical Society. 131, 3152–3153 (2009).

[10]. Liu, S., Yu, J. & Jaroniec, M. Anatase TiO2 with Dominant High-Energy 001 Facets: Synthesis, Properties, and Applications. Chemistry of Materials. 23, 4085–4093 (2011).

[11]. Liu, B. et al. Highly dispersive {001} facets-exposed nanocrystalline TiO2 on high quality graphene as a high performance photocatalyst. Journal of Materials Chemistry. 22, 7484–7491 (2012).

[12]. Feng W, Sun E, Fujii A, Wu H, Niihara K, et al. (2000) Synthesis and characterization of photoconducting polyaniline-TiO2 nanocomposites. Bull Chem Soc Jpn 73: 2627–2633.

[13]. Li X, Chen W, Bian C, He J, Xu N, et al. (2003) Surface modification of TiO2 nanoparticles by polyaniline. Appl Surf Sci 217 : 16–22.

[14]. Li J, Zhu L, Wu Y, Harima Y, Zhang A, et al. (2006) Hybrid composites of conductive polyaniline and nanocrystalline titanium oxide prepared via self-assembling and graft polymerization. Polymer 47: 7361–7367.

[15]. Drew C, Liu X, Ziegler D, Wang X, Bruno FF, et al. (2003) Metal oxide-coated polymer nanofibers. Nano Lett 3: 143–147.

[16]. Kedem S, Schmidt J, Paz Y, Cohen Y (2005) Composite polymer nanofibers with carbon nanotubes and titanium dioxide particles. Langmuir 21: 5600–5604.
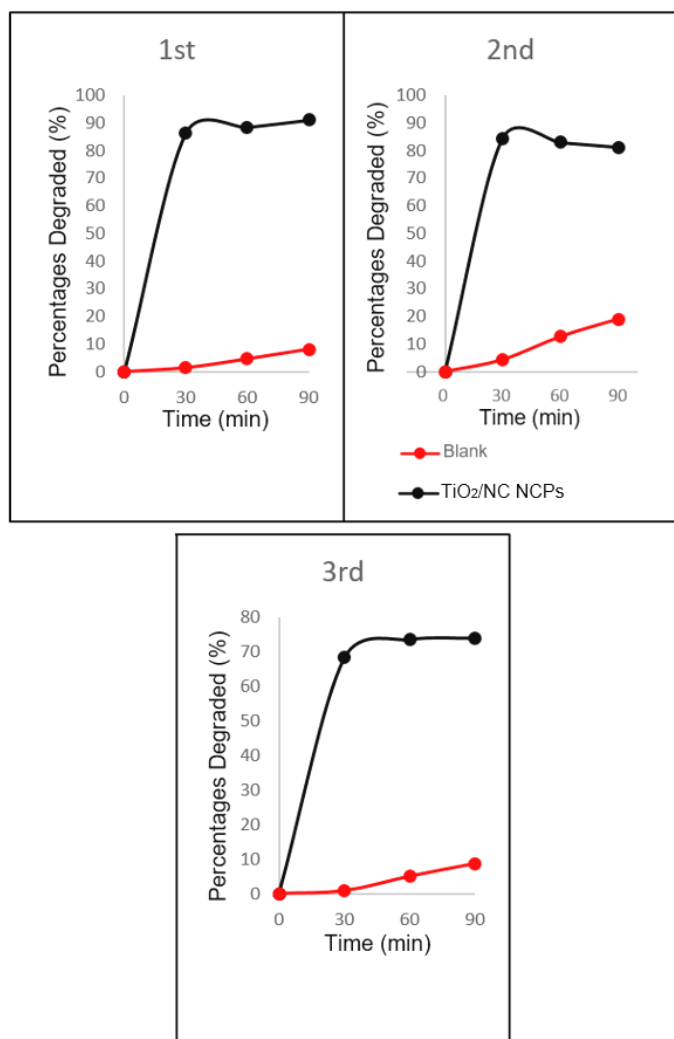
[17]. Banerjee S, Wong SS (2002) Synthesis and characterization of carbon nanotube-nanocrystal heterostructures. Nano Lett 2: 195–200.

[18]. Sun Z, Kim D, Wolkenhauer M, Bumbu G, Knoll W, et al. (2006) Synthesis and photoluminescence of titania nanoparticle arrays templated by block-copolymer thin films. Chem Phys Chem 7: 370–378.

[19]. Bartl MH, Boettcher SW, Frindell KL, Stucky GD (2005) 3-D molecular assembly of function in titania-based composite material systems. Acc Chem Res 38: 263–271.

[20]. Coakley KM, McGehee MD (2003) Photovoltaic cells made from conjugated polymers infiltrated into mesoporous titania. Appl Phys Lett 83: 3380–3382.

[21]. Zhang M, Gao G, Li C, Liu F (2004) Titania-coated polystyrene hybrid microballs prepared with miniemulsion polymerization. Langmuir 20: 1420–1424.

[22]. Caruso RA, Susha A, Caruso F (2001) Multilayered titania, silica, and laponite nanoparticle coatings on polystyrene colloidal templates and resulting inorganic hollow spheres. Chem Mater 13: 400–409.

[23]. Kwak S, Kim SH, Kim SS (2001) Hybrid organic/inorganic reverse osmosis (RO) membrane for bactericidal anti-fouling. 1. Preparation and characterization of TiO2 nanoparticle self-assembled aromatic polyamide thin-film-composite (TFC) membranes. Environ Sci Technol 35 : 2388–2394.

[24]. Chen WC, Lee SJ, Lee LH, Lin JL (1999) Synthesis and characterization of trialkoxysilane-capped poly(methyl methacrylate)-titania hybrid optical thin films. J Mater Chem 9: -.

[25]. Davis SA, Breulmann M, Rhodes KH, Zhang B, Mann S (2001) Template-Directed assembly using nanoparticle building blocks: A nanotectonic approach to organized materials. Chem Mater 13: 3218–3226.

[26]. Lee LH, Chen WC (2001) High-refractive-index thin films prepared from trialkoxysilane-capped poly(methyl methacrylate)titania materials. Chem Mater 13: 1137–1142.

[27]. Schmidt H, Jonschker G, Goedicke S, Mennig M (2000) The sol-gel process as a basic technology for nanoparticle-dispersed inorganic-organic composites. J Sol-Gel Sci Technol 19: 39–51.

[28]. Yoshida M, Lal M, Kumar N, Prasad P (1997) TiO2 nano-particle-dispersed polyimide composite optical waveguide materials through reverse micelles. J Mater Sci 32: 4047–4051.

[29]. Ng C, Ash B, Schadler L, Siegel R (2001) A study of the mechanical and permeability properties of nano-and micron-TiO2, filled epoxy composites. Adv Comp Lett 10: 101–111.

[30]. Sasaki T, Ebina Y, Tanaka T, Harada M, Watanabe M, et al. (2001) Layer-by-layer assembly of titania nanosheet/polycation composite films. Chem Mater 13:4661–4667.

[31]. Alexandre M, Dubois P (2000) Polymer-layered silicate nanocomposites: preparation, properties and uses of a new class of materials. Mater Sci Eng R 28: 1–63.

[32]. Ray SS, Okamoto M (2003) Polymer/layered silicate nanocomposites: a review from preparation to processing. Prog Polym Sci 28: 1539–1641.

[33]. Michael Ioelovich (2012), Study of Cellulose Interaction with Concentrated Solutions of Sulfuric Acid, ISRN Chemical Engineering Volume 2012, Article ID 428974, 7 pages doi:10.5402/2012/428974.

[34]. E. N. J. Ford, S. K. Mendon, S. F. Thames and J. W. Rawlins, (2010) "X-ray Diffraction of Cotton Treated with Neutralized Vegetable Oil-based Macromolecular Crosslinkers," Journal of Engineered Fibers and Fabrics, 5(1): 14.

[35]. S. Park, J. O. Baker, M. E. Himmel, P. A. Parilla and D. K. Johnson, (2010) "Cellulose crystallinity index: measurement techniques and their impact on interpreting cellulase performance," Biotechnology for Biofuels, 3(10): 2-4.

[36]. Troedec, M., Sedan, D., Peyratout, C., Bonnet, J., Smith, A., Guinebretiere, R., Gloaguen, V., and Krausz, P., "Influence of various chemical treatments on the composition and structure of hemp fibers", Composites Part A-Appl. Sci. Manufact., 39, 514- 522, 2008.

[37]. Mandal, A., and Chakrabarty, D., "Isolation of nanocellulose from waste sugarcane bagasse (SCB) and its characterization", Carbohydr. Polym, 86, 1291-1299, 2011.

[38]. Garside, P., and Wyeth, P., "Identification of cellulosic fibres by FTIR spectroscopy: Thread and single fibre analysis by attenuated total reflectance", Stud. Conser, 48, 269-275, 2003.

[39]. Nelson, M. L., and O'Connor, R. T., "Relation of certain infrared bands to cellulose crystallinity and crystal lattice type. Part I. Spectra of lattice types I, II, III and amorphous cellulose", J. Appl. Polym. Sci., 8, 1311-1324, 1964.

[40]. Nelson, M. L., and O'Connor, R. T., "Relation of certain infrared bands to cellulose crystallinity and crystal lattice type. Part II. A new infrared ratio for estimation of crystallinity in cellulose I and II", J. Appl. Polym. Sci., 8, 1325-1341, 1964.

[41]. Anuj Kumar and et al (2014), Characterization of Cellulose Nanocrystals Produced by Acid-Hydrolysis from Sugarcane Bagasse as Agro-Waste, Journal of Materials Physics and Chemistry, Vol. 2, No. 1, 1-8.